# Reversible Tuning of Ca Nanoparticles Embedded in a Superionic $CaF_2$ Matrix

J. Ruiz-Fuertes,[*,†] J. Ibáñez,[‡] V. Monteseguro,[¶] I. Alencar,[§] and C. Cazorla[‖]

†*DCITIMAC, Universidad de Cantabria, Avenida de Los Castros 48, 39005 Santander, Spain*

‡*Institute of Earth Sciences Jaume Almera, ICTJA-CSIC, Lluís Solé i Sabarís s/n, 08028 Barcelona, Spain*

¶*Departamento de Física Aplicada, Universitat de València, Dr. Moliner 50, 46100 Valencia, Spain*

§ *Instituto de Física, Universidade Federal do Rio Grande do Sul, Avenida Bento Gonçalves 9500, CEP 91501-970 Porto Alegre-RS, Brazil*

‖*School of Materials Science and Engineering, UNSW Australia, Sydney NSW 2052, Australia*

E-mail: ruizfuertesj@unican.es

**Abstract**

Controlling the size and shape of metallic colloids is crucial for a number of nanotechnological applications ranging from medical diagnosis to electronics. Yet, achieving tunability of morphological changes at the nanoscale is technically difficult and the structural modifications made on nanoparticles generally are irreversible. Here, we present a simple non-chemical method for controlling the size of metallic colloids in a reversible manner. Our strategy consists on applying hydrostatic pressure on a Ca cationic sublattice embedded in the irradiated matrix of $CaF_2$ containing a large concentration of defects. Application of our method to $CaF_2$ along with *in situ* optical absorption of the Ca plasmon shows that the radii of the Ca nanoparticles can be reduced with an almost constant rate of $-1.2$ nm/GPa up to a threshold pressure of $\sim 9.4$ GPa. We demonstrate recovery of the original nanoparticles upon decompression of the irradiated matrix. The mechanisms for reversible nanocolloid-size variation are analyzed with first-principles simulations. We show that a pressure-driven increase in the binding energy between fluorine centers is responsible for the observed nanoparticle shrinkage. We argue that the same method can be used to generate other metallic colloids (Li, K, Sr, and Cs) with tailored dimensions by simply selecting an appropriate matrix.

# Introduction

Metal nanoparticles (MNP) are the pillar of many technological applications extending from calorimetric sensors and chemical catalysts to *in vivo* imaging and photothermal therapy[1]. The success of these technologies strongly depend on the shape and size of the MNP. However, achieving specific modifications on the morphology of MNP can be an arduous and erratic task when chemical methods are used[2,3]. Additionally, the structural changes inflicted on MNP by synthetic methods normally are permanent, which hinders the reutilization of expensive products based on nanocolloids. An extreme case occurs when MNP are embedded

in composite materials involving dielectric matrices, which is a common setup in plasmonic applications[4]; subsequent size tuning of the entreched MNP is unattainable with current methods.

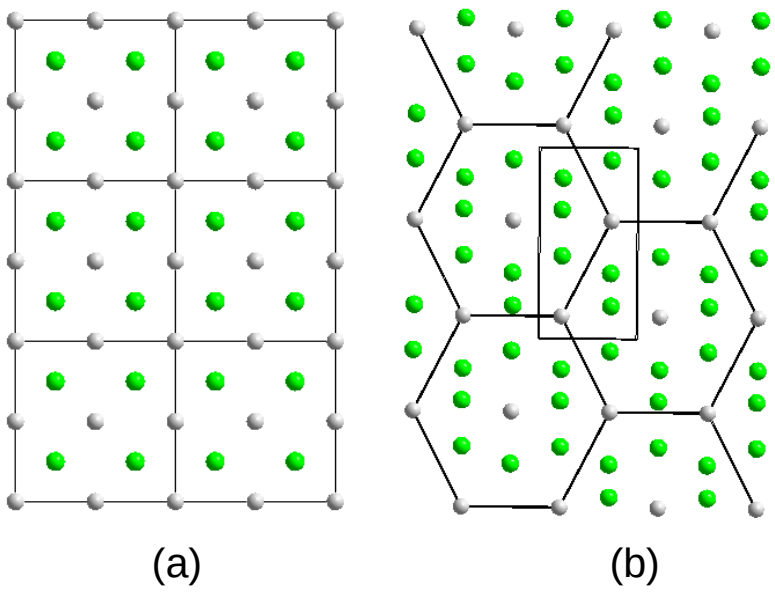


Figure 1: (a) Crystal structure of fluorite $CaF_2$ in which the Ca cationic lattice coincides with that of *fcc* metallic calcium. (b) Cystal structure of the high-pressure contunnite $CaF_2$ structure in which the Ca cations are arranged in a *hcp* sublattice. Ca and F atoms are represented with white and green spheres, respectively. The cationic lattice is highlighted with solid lines. In (a) the cationic lattice coincides with the unit-cell edges but in (b) they are represented by the rectangle.

Here we present a simple and effective physical method to reversibly tune the size of Ca MNP. Our method consists of applying hydrostatic pressure on Ca MNP embedded in a dielectric matrix, which are generated by irradiating a crystal; in this way, a large concentration of highly mobile point defects is created. We apply our method to control the size of calcium nanoparticles in $CaF_2$ (Ca@$CaF_2$). Our starting point is a $CaF_2$ crystal irradiated with 2.2 GeV $^{197}$Au ions[5] (other irradiation techniques involving x-rays or different types of ions[6], or simple exposure to ultraviolet light, to metal vapor, or electron beam lithography[7], should also provide an alternative means to fabricate similar nanostructures[8–10]); the irradiated matrix contains a large number of highly mobile fluorine vacancies and interstitials[11–16],

hence calcium nanoparticles with a crystal symmetry compatible with that of $CaF_2$ naturally appear (Fig.1a). Here, we show that subsequent application of hydrostatic pressure causes the radii of the so-generated MNP to decrease considerably in a controlled and reversible manner. Specifically, using *in situ* optical absorption spectroscopy we determine that the radii of the Ca nanoparticles are reduced at an almost constant rate of $-1.2$ nm/GPa up to a pressure of $\sim 9.4$ GPa, when a structural phase transition occurs in $CaF_2$ (Fig.1) and the MNP vanish. The proposed MNP modification method red under high pressure exploits the appearance of metallic clusters and color centers in dielectric matrices, which usually are regarded as a drawback for classical-optics applications[17–20], to engineer new functional materials.

## Experimental Details

Irradiated high-purity $CaF_2$ single crystals from the Optical Institute (St. Petersburg, Russia) were employed. The irradiation with ions was performed in vacuum at the linear accelerator UNILAC (GSI, Darmstadt, Germany) with 2.2 GeV $^{197}$Au ions at ambient temperature, the ion flux was kept to $10^8$–$10^9$ ion/cm$^2$s with a fluence of $2\times10^{11}$ ions/cm$^2$. More details can be found in Ref.[5]. For optical absorption in the UV-VIS range, $\sim$15 $\mu$m thick single crystals were cleaved and placed together with a ruby chip for pressure determination[42] into the 200 $\mu$m hole drilled in a 50 $\mu$m thick stainless steel gasket inserted between two IIA diamonds of a membrane-type diamond anvil cell (DAC). The transmittance measurements were carried out with a confocal optical setup that consisted of a deuterium lamp, fused silica lenses, two Cassegrain objectives, and two UV-VIS spectrometers to cover the measured range. The surface area of the sample was around $80\times60$ $\mu$m$^2$ and the focused beam spot was of 25 $\mu$m in diamater.

## Calculations Details

First-principles calculations were performed with the VASP code[43] by using the generalized gradient approximation to the exchange-correlation energy due to Perdew *et al.*[44] The projector augmented-wave method is used to represent the ionic cores,[45] and the Ca's $6p$-$2s$, and F's $2s$-$5p$ electronic states are considered as valence band states. Wave functions are represented in a plane-wave basis truncated at 650 eV. By using these parameters and dense **k**-point grids for integration within the Brillouin zone (equivalent to a $16 \times 16 \times 16$ mesh employed for the cubic fluorite structure), the resulting energies are converged to within 1 meV per formula unit. In the geometry relaxations, a threshold tolerance of 0.01 eV/Å is imposed on the atomic forces.

The binding energy between F centers has been estimated with the formula[10]

$$\begin{aligned} E_{\rm bind}(P) &= \frac{1}{64}\left[E_{\rm Ca_{32}}(P) + 63E_{\rm Ca_{32}F_{64}}(P)\right] - \\ & E_{\rm Ca_{32}F_{63}}(P)\ , \end{aligned} \tag{1}$$

where the first term in the rhs of (1) corresponds to the energy of bulk *fcc* Ca, the second to the energy of bulk fluorite $CaF_2$, and the third to the energy of non-stoichiometric bulk fluorite $CaF_2$ for a given pressure $P$; the subscripts indicate the size of the supercells that have been employed to compute each energy term (e.g., $Ca_{32}F_{63}$ represents a 32-formula unit fluorite $CaF_2$ supercell in which one F ion has been removed).

The interface energy per unit surface of a *fcc* Ca nanoparticle embedded in a fluorite $CaF_2$ matrix can be estimated with the formula[10]

$$\begin{aligned} E_{\rm interface}(P) &= E_{\rm Ca_{n/2}F_n|Ca_m|Ca_{n/2}F_n}(P) - \\ & E_{\rm Ca_m}(P) - E_{\rm Ca_nF_{2n}}(P)\ , \end{aligned} \tag{2}$$

where "$Ca_{n/2}F_n|Ca_m|Ca_{n/2}F_n$" stands for a supercell constructed by stacking $m$ *fcc* Ca unit cells on top of $n$ fluorite $CaF_2$ unit cells and in which periodic boundary conditions are applied along the three Cartesian directions. The lattice parameter of bulk $CaF_2$ is constrained along the stacking direction; this can be done because the arrangement of Ca atoms in the nanoparticle and fluorite $CaF_2$ is the same, and the stiffness of $CaF_2$ is significantly larger than that of Ca (hence we assume that the colloid completely takes up the mechanical stress). The energy penalty associated to the mechanical strain of the nanoparticle is considered separately (see below). In order to avoid spurious interactions between periodic interface images, the size of the supercell along the stacking direction needs to be sufficiently large. We have performed tests on the convergence of the $E_{Ca_{n/2}F_n|Ca_m|Ca_{n/2}F_n}$ energy with respect to the supercell size and concluded that parameters $m = 3$ and $n = 11$ provide sufficiently accurate results converged to within 10 meV/nm$^2$.

Finally, the stress energy per unit volume of a *fcc* Ca nanoparticle embedded in a fluorite $CaF_2$ matrix is calculated as[10]

$$E_{\text{strain}}(P) = \int \sigma d\epsilon = \frac{3}{2} B(P) \epsilon^2(P) \ , \tag{3}$$

where $B$ represents the bulk modulus of bulk *fcc* Ca and $\epsilon \equiv \frac{a_{Ca} - a_{CaF_2}}{a_{CaF_2}}$ the accompanying lattice strain for a given pressure $P$.

# Results and Discussion

At ambient conditions, the interaction of light with calcium colloids in irradiated $CaF_2$ produces a broad absorption band located at around 560 nm (Fig.2), which can be modelled as a function of colloid size by using Mie theory[21–23]. In order to *in situ* monitor the size of the calcium colloids in $CaF_2$ under high pressure, we employ optical absorption spectroscopy. This technique is widely used to quantify the number of MNPs in ionic crystals and can be performed inside the diamond anvil cell. The experimental data are analyzed by Mie

theory assuming that the calcium nanoparticles are spherical, and *ab initio* simulations are performed to disclose the atomistic mechanisms causing the MNP size reduction.

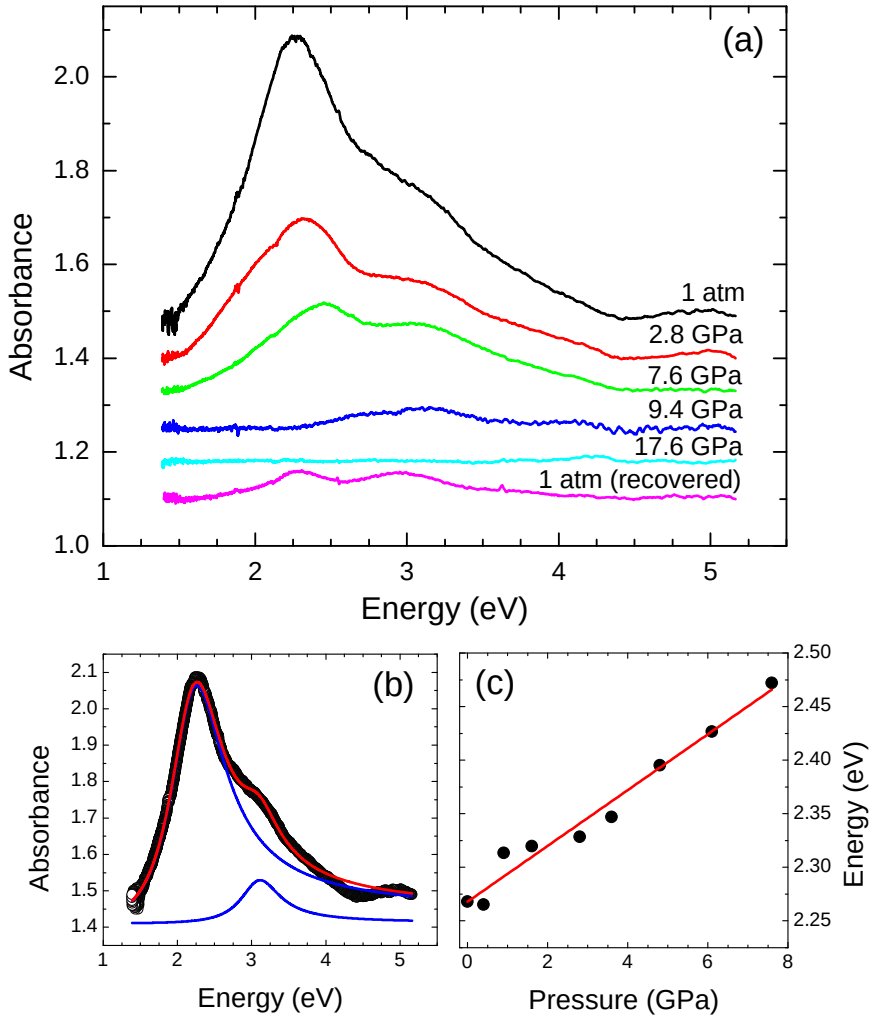


Figure 2: (a) Optical absorption spectra of $CaF_2$ at different pressures. (b) Lorentzian fit of the spectrum at ambient pressure. (c) Pressure dependence of the broad and intense absorbance band of $CaF_2$ due to the absorption of Ca colloids. The experimental data and fits are represented by points and continuous red lines, respectively, in (b) and (c).

A summary of the absorption spectra obtained at different pressures is shown in Fig. 2. The absorbance spectrum of irradiated $CaF_2$ at ambient pressure is well known and consists of two bands (Fig.2 (b)). The first band, located at 2.28 eV (545 nm), is a relatively intense broad band that normally is attributed to the presence of Ca colloids[24]. The second band is a narrower and weaker band located at 3.25 eV (382 nm) that is attributed to the presence of F-centers[25]. Under pressure, the overall absorbance reduces and the maximum of the broad

band blueshifts at a rate of 0.025 eV/GPa (Fig.2c). At $P = 9.4$ GPa, the absorption spectrum changes drastically and the intensity of the first peak drops abruptly. Such an intensity reduction is most probably related to a noticeable decrease in the density of colloids under pressure confirmed by the complete dissapearence of the bands at higher pressures. However, when pressure is released both bands reappear (although their absorbance intensities are much lower). The disappearance of the bands above 9.4 GPa can be associated with the pressure-induced phase transition[26] that $CaF_2$ undergoes at this pressure from the fluorite (space group $Fm\bar{3}m$) to the contunnite phase (space group $Pnma$), as shown in Fig. 1. We will elaborate on the causes of this effect latter on when explaining our *ab initio* calculations.

To a first approximation, and due to their small size, let us assume that the optical properties of the Ca@$CaF_2$ colloids can be described within the Rayleigh limit, a good approximation when the size of the MNPs is much smaller than the wavelength of light. In this case, the resonance in the total absorption cross-section of the system is expected to occur when

$$\epsilon(\omega) = -2\epsilon_m \ , \tag{4}$$

where $\epsilon(\omega)$ and $\epsilon_m$ are the dielectric functions of metallic calcium and the surrounding $CaF_2$ medium, respectively. Considering that the pressure coefficient of the refracive index of $CaF_2$ is very small ($2.44 \times 10^{-3}$ $GPa^{-1}$)[28], $\epsilon_m$ can be assumed to be independent of wavelength and pressure while $\epsilon(\omega)$ can be expressed by using the Drude model, which neglects interband transitions and the finite lifetime of the plasmons, i.e. $\epsilon(\omega) = 1 - \omega_p^2/\omega^2$ (where $\omega_p^2 = 4\pi Ne^2/m^*$ is the plasma frequency of the bulk metal, and $N$ and $m^*$ the density and effective mass of the conduction electrons, respectively). According to Rayleigh's condition, the resonance takes place when

$$\omega = \omega_p/\sqrt{1 + 2\epsilon_m} \ . \tag{5}$$

Using the value $m^* = 1.9m_e$ for the optical mass of the electrons in bulk Ca, the resulting plasma frequency for Ca is 5.78 eV.[22] By using these values and Eq. 5, it is found that the resonance frequency for Ca@$CaF_2$ nanocolloids should occur at 2.56 eV, which is close to the maximum absorbance measured in our sample at ambient pressure (2.28 eV, see Fig. 2). Thus, the Rayleigh approximation provides a reasonable estimation of the wavelength of the maximum absorbance in these colloids.

The pressure behavior of the optical properties of the Ca@$CaF_2$ system can then be obtained analytically from Eq. 5 by taking its pressure derivative

$$d\omega/dP = (\omega_p/2B_0)/\sqrt{1+2\epsilon_m}\ , \tag{6}$$

where $B_0$ is the bulk modulus of the Ca nanocolloids (which appears after taking the pressure derivative of $N$). The degree of compression of the Ca nanocolloids should be dictated by the less compressible $CaF_2$ matrix, hence it can be assumed that $B_0$ is equal to the bulk modulus of $CaF_2$, namely, 82 GPa.[27] By using this value and Eq. 6, one finds that the pressure coefficient expected for the plasmon resonance within the Rayleigh limit is 0.015 eV/GPa, which is significantly smaller than the experimental value of 0.025 eV/GPa. The difference between these theoretical results and the experiments becomes even larger when the pressure behavior of the $CaF_2$ refractive index[28] is taken into consideration in the analysis: the pressure coefficient deduced in this case becomes $\sim 4$ meV/GPa larger. In spite of the possible limitations of the presented simple approach based on the Rayleigh's limit, the large differences between theory and experiments suggest that an overlooked effect may be modifying the pressure dependence of the optical absorbance of Ca@$CaF_2$ colloids. As we will show next, such a difference can be explained in terms of a pressure-induced shrinkage of the colloids.

A better description of the pressure behavior of the optical absorbance of the Ca@$CaF_2$ colloids can be obtained with Mie theory.[10,22] In the present work we employ the software MiePlot,[29] which is based on the classical work by Bohren and Huffman,[30] and closely follow

the procedure used by Orera and Alcalá to simulate the optical properties of Ca@$CaF_2$ spherical colloids at ambient conditions.[22] Within this approach, the dielectric function of the metal is modeled through the Drude function, including the finite lifetime of the plasmons and interband terms that, for the sake of simplicity, here are assumed to be independent of pressure. An additional correction on the plasmon damping due to the small particle size of the colloids has been taken into account.[22] In the present calculations, the dielectric functions and spherical sizes of metallic Ca nanocolloids were obtained at different pressures by assuming that the pressure dependence of the corresponding dielectric function stems from changes in the electron density, a good approximation within the Drude model; the bulk modulus of $CaF_2$ was employed, as justified previously. The pressure dependence of the refractive index of $CaF_2$ is also included in our analysis by following the work of Schmidt and Vedam[28]. It is worth noting that test calculations of the extinction efficiency performed for vanishingly small particle sizes at ambient pressure, $Q_{\rm ext}$, are in very good agreement with those obtained analytically with the Rayleigh approximation (Eq.5).

Fig. 3 shows the experimental absorbance (solid curves) and $Q_{\rm ext}$ calculated with Mie theory (dashed curves) at two different pressures (1 atm and 6.1 GPa). As can be seen in the figure, the theoretical curves qualitatively follow the wavelength dependence of the absorbance maxima. At ambient pressure, the best agreement between the experimental absorbance and $Q_{\rm ext}$ is obtained by considering a radius $R$ of 31 nm for spherical Ca colloids. At $P = 6.1$ GPa, the particle size that is found to better reproduce the experimental curve is 23 nm. These values are of the same order of magnitude as those reported by Rix *et* al. for $CaF_2$ crystals irradiated with intense UV light.[10]

Fig. 4 shows the pressure-dependence of the particle size of the Ca colloids as extracted from the analysis of the absorbance curves with Mie theory. As can be seen therein, the size of the nanocolloids is approximately reduced at a constant rate of $-1.2$ nm/GPa over the entire pressure range. By performing similar calculations at different particle sizes and constant pressure, it can be shown that such a size reduction leads to a $\sim 0.014$ eV/nm

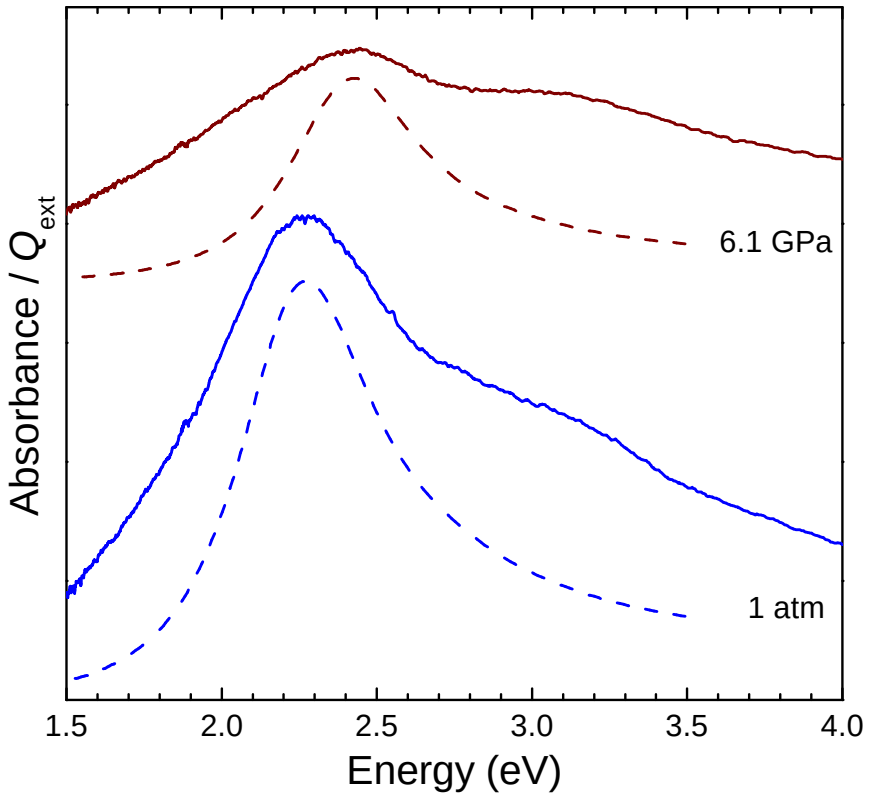


Figure 3: Experimetal (continuous line) and calculated by Mie theory (dashed line) absorbance spectra of irradiated $CaF_2$ at ambient temperature and $P = 1$ atm and 6.1 GPa.

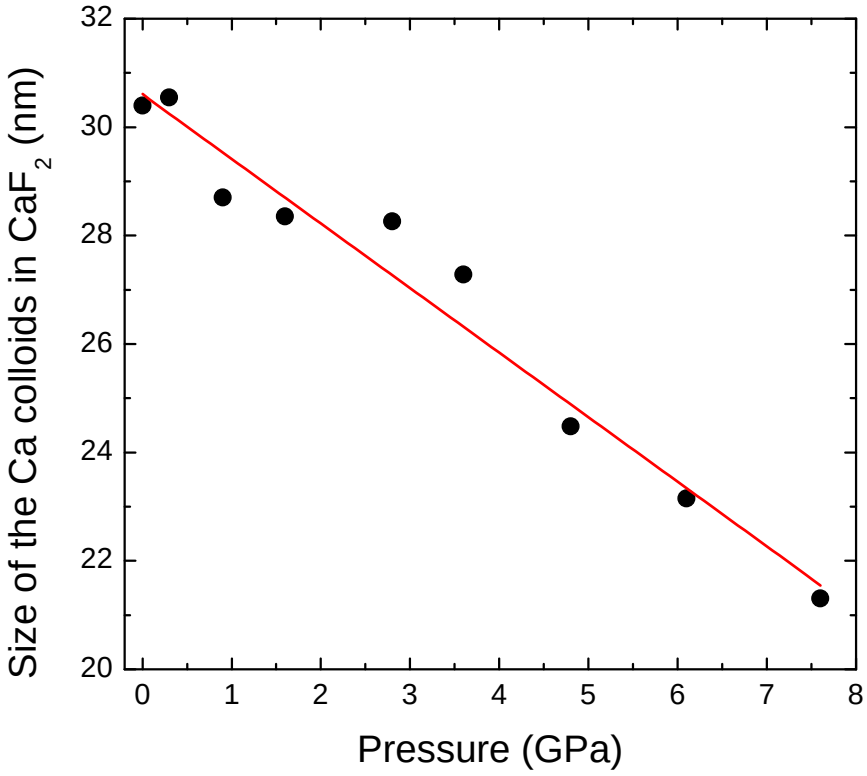


Figure 4: Pressure-dependence of the Ca colloids radius in $CaF_2$. Results are obtained by approximating the calculated extinction spectra with Mie theory to the experimental absorbance spectra. The fit (continuous line) yields a size reduction of $\mathrm{d}R/\mathrm{d}p = -1.2$ nm/GPa.

increase in the absorbance maximum at zero pressure. At around 6 GPa, this value decreases down to $\sim 0.011$ eV/nm. Consequently, the pressure coefficient of the absorbance maxima is enhanced by 0.013–0.017 eV/GPa due to a pressure-induced size reduction, regardless of the shifts arising from the increase in $N$ under pressure. As shown previously in the description of the optical properties of Ca@$CaF_2$ colloids within the Rayleigh limit, such an increase can account for around half of the experimental pressure coefficient (0.025 eV/GPa). The remaining part, as predicted by the Rayleigh limit ($\sim 0.011$ eV/GPa), is originated by the increase of $N$ upon compression. Hence, our analysis based on Mie theory provides an explanation for the fast blueshift observed in the Ca colloidal band.

In order to analyze the mechanisms of the formation of Ca nanoparticles in irradiated $CaF_2$ and their pressure-induced shrinkage, we focus on the binding of F centers, since it can be related to the formation of the Ca colloids in $CaF_2$. We perform first-principles calculations based on density functional theory (DFT). Following the previous work by Rix et al. [10], we express the formation energy of a spherical metal nanoparticle as:

$$E_{\text{colloid}} = E_{\text{bind}} + E_{\text{interface}} + E_{\text{strain}} \ , \tag{7}$$

where the first term in the rhs of Eq. (7) accounts for the binding between F centers (or vacancies), the second for the energy associated to the creation of the colloid interface, and the third for the distortion energy resulting from the lattice mismatch between the metal nanoparticle and surrounding $CaF_2$ matrix. Normally, $E_{\text{bind}}$ favors the formation of colloids whereas $E_{\text{interface}}$ and $E_{\text{strain}}$ prevent it.

Figure 5 shows the dependence of the colloid formation energy and the components $E_{\text{bind}}$, $E_{\text{interface}}$, and $E_{\text{strain}}$ on the nanoparticle radius, $R$, and pressure Calculation Details Section). At equilibrium (Fig. 5a), we compute a binding energy between F centers of $-47.35$ eV/nm$^3$ (or, equivalently, of $-0.99$ eV per fluorine vacancy), an interface colloid energy of 3.24 eV/nm$^2$, and a strain colloid energy of 0.002 eV/nm$^3$. In this case, the minute-

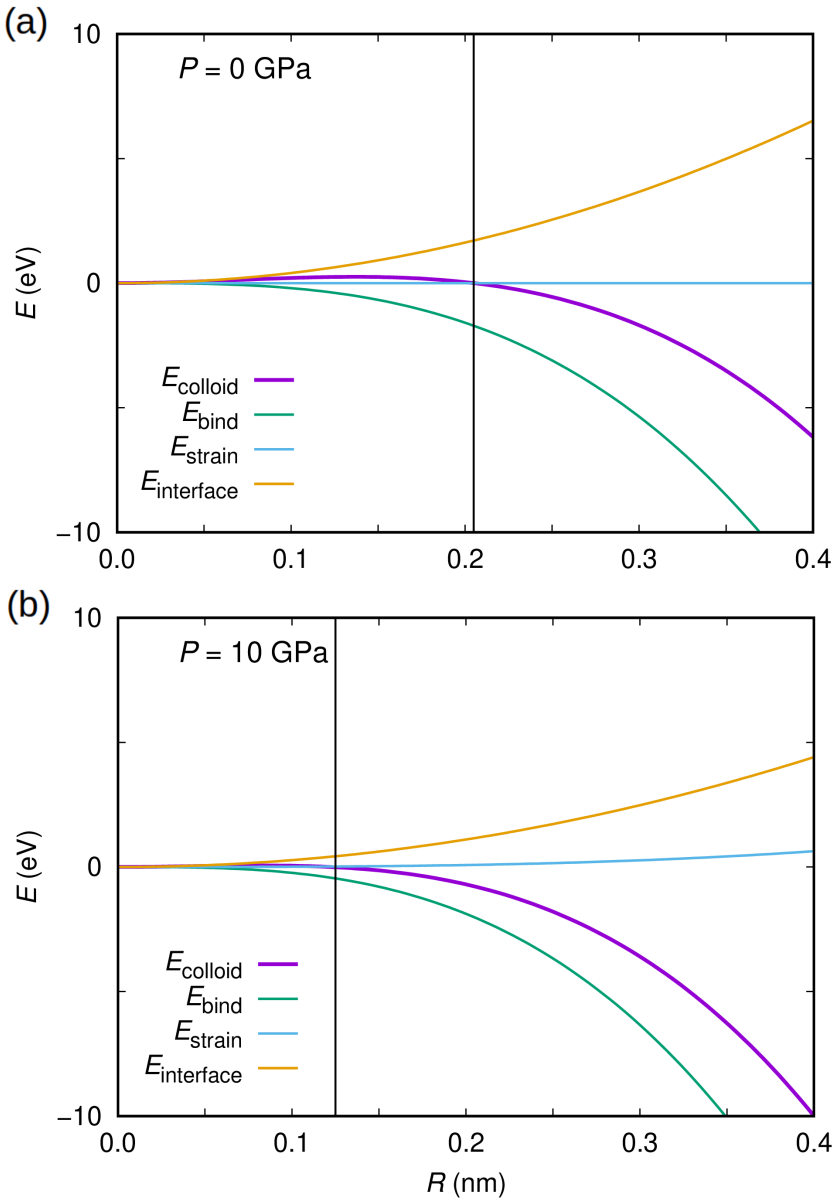


Figure 5: First-principles calculations of the formation energy of Ca colloids in irradiated $CaF_2$ at (a) zero pressure and (b) 10 GPa. The $R$-dependence of the different $E_{\text{colloid}}$ contributing terms are shown. The vertical black lines in the figures indicate the minimum threshold radii for energetically favorable formation of nanoparticles, $R_{\text{min}}$.

ness of the $E_{\rm strain}$ term is due to the practically coincident equilibrium lattice parameters of bulk *fcc* Ca and fluorite $CaF_2$ (Methods Section). The formation of Ca colloids is energetically favorable for radii larger than $R_{\rm min}(0) = 0.21$ nm owing to the dominant role of the $E_{\rm bind}$ term at such lengths. Under compression (Fig. 5b), the bind and interface colloid energies decrease (e.g., $E_{\rm bind} = -56.07$ eV/nm$^3$ and $E_{\rm interface} = 2.19$ eV/nm$^2$ at $P_m = 10$ GPa) while the colloid strain energy increases due to the increase in the lattice mismatch between the *fcc* nanoparticle and surrounding fluorite matrix (e.g., $E_{\rm strain} = 2.36$ eV/nm$^3$ at $P_m$). Nevertheless, the $P$-driven raise in strain energy is not able to counteract the steadily more attractive binding between F centers and consequently the threshold radius $R_{\rm min}$ decreases under pressure; for instance, we estimate a $R_{\rm min}$ of 0.19 nm at 5 GPa and of 0.13 nm at $P_m$.

The $E_{\rm colloid}$ theory that we employ here assumes an infinite source of F centers, which is a highly idealized picture of the real system (in practice the number of F centers is limited by the amount of received radiation and occurrence of recombination events with $F_2^-$ dimers). Consequently, we are not able to calculate an optimal or average Ca nanoparticle radius as a function of pressure. Nevertheless, it can be reasonably assumed that such an optimal or average colloid radius, $R_{\rm opt}$, will follow a similar pressure-induced variation than $R_{\rm min}$ since the average number of F centers per colloid will remain roughly constant owing to the energy barriers involved in ionic diffusion (which typically increase under pressure[31,32]); therefore, based on our DFT calculations, we estimate that at $P_t = 8$ GPa $R_{\rm opt}$ will shrink by $\sim 25\%$ of its equilibrium value. This theoretical prediction is in good agreement with our experimental observation that the size of Ca colloids decreases by $\sim 30\%$ when increasing pressure from ambient to the fluorite $\rightarrow$ contunnite transition point (see Fig. 4), which comes to validate our energy arguments explained above. Meanwhile, the likely reasons for the disappearance of Ca colloids at pressures $P_t < P$ are (1) the lack of superionicity in the contunnite phase of $CaF_2$,[32,33] which prevents the coalescence of F centers, and (2) the large energy penalty involved in the creation of a *fcc* Ca/contunnite $CaF_2$ interface owing to the very distinct arrangements of Ca ions in the two structures[34].

The dissipation of Ca nanoparticles at the pressure point at which $CaF_2$ undergoes a phase transition from a cubic to an orthorhombic phase, illustrates the fact that our MNP size tuning technique cannot be generalized to any material. In particular, the crystal symmetry of the metallic sublattice within the matrix and the resulting MNP need to be coincident (*fcc* in the present case). Moreover, in order to guarantee the initial formation of nanocolloids at ambient temperature within the matrix, the lattice mismatch between the metallic sublattice and the MNP must be small. Otherwise, the formation of anion centers dominates and the resulting MNP are amorphous and most likely to be unstable under high pressure[35]. This is the case, for instance, for heavily irradiated NaCl in which metallic Na is *bcc* and the matrix Na@NaCl is *fcc*. This forces Na to keep an unstable *fcc* arrangement.

Figure 6 shows a number of binary ionic compounds in which superionicity has been observed, or is very likely to occur,[32,36] and the structural symmetry requirement explained above is fulfilled. Among those compounds, LiF, $SrF_2$ and CsF also fulfill the second requirement that $a$ (compound) $\approx$ $a$ (metal) (in the case of LiF above 7 GPa)[37]. Therefore, Li, Sr, and Cs MNP with customized radii in principle could be also produced with pressure-based techniques. Moreover, pressure-induced quenching could be exploited to accomplish further MNP radius control. For instance, bulk Li crystallizes in a *bcc* structure whereas in LiF, LiCl, LiBr, and LiI, lithium renders a *fcc* sublattice; however, at $\sim$ 7 GPa Li transforms[37] from *bcc* to *fcc* with an almost identical lattice parameter to LiF, hence the appearance of Li MNP is expected beyond that point. In this particular case, pressure-induced quenching could be used to achieve control of the Li MNP radius at pressures below $\sim$ 7 GPa. Exactly the same would occur for KF in which K undergoes a *bcc* to *fcc* transition[38] at 12.4 GPa. Likewise, Sr undergoes a *fcc* to *bcc* phase transition[39] at 4.2 GPa. In this case, the stress due to lattice mismatch could quench Sr MNP in $SrF_2$ and $SrCl_2$ at pressures beyond that transition point. Meanwhile, the case of CsF is almost identical to $CaF_2$. CsF transforms from *fcc* to a cubic structure (space group $Pm\bar{3}m$) with a simple cubic cationic lattice at 4.8 GPa[40]; however, at ambient temperature Cs displays a *fcc* structure that is stable up to

88 GPa[41] hence Cs MNP are likely to vanish at $P > 4.8$ GPa.

In order to fulfill the lattice parameter requirement $a$ (compound) $\approx a$ (metal), doping strategies based on isoelectronic element substitutions may be used; in this way the electronic features of the system would not be affected while potentially improving their structural and superionic properties[32]. Biaxial and uniaxial stresses could lead to similar control of MNP radii as demonstrated here. An additional feature is that negative stresses, inducing an increase in the dimensions of the nanocolloids formed at equilibrium, can be applied effectively[31].

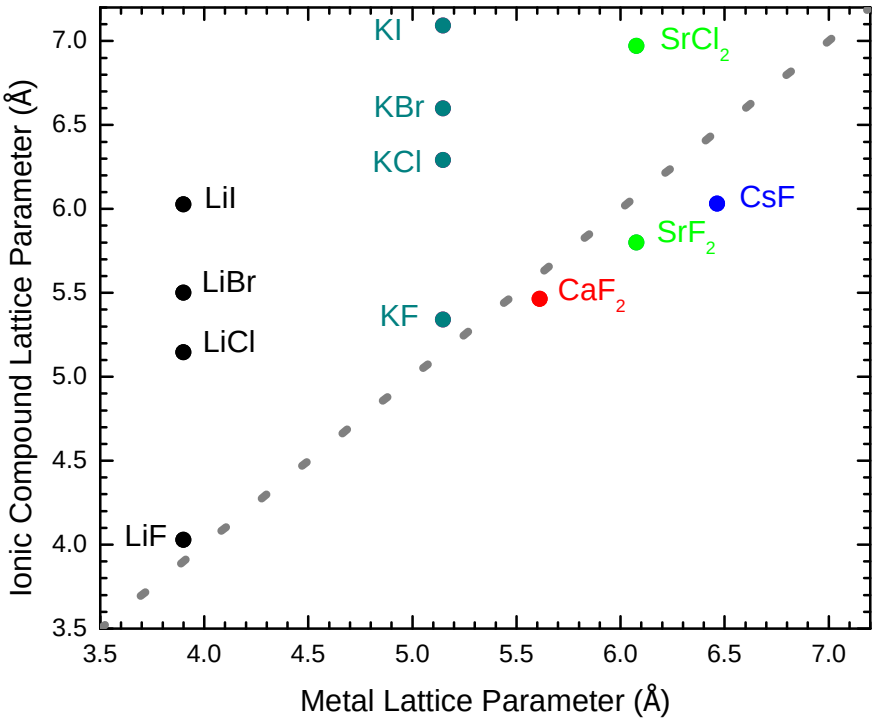


Figure 6: The lattice parameter of binary *fcc* ionic compounds versus the lattice parameter of the corresponding bulk *fcc* metals. In *bcc* or *hcp* structured binary ionic crystals there is no structural correspondence with the structure of their corresponding metallic cations. The discontinuous line represents an ideal zero lattice strain between both lattice parameters.

# Conclusions

In conclusion, we have found a non-chemical method for reversibly controlling the size of metallic colloids embedded in the cationic sublattice of an irradiated crystal. Contrary to conventional synthetic procedures in which the production of size-controlled metallic nanoparticles is non-reversible, the high-pressure method introduced here allows us to reversibly tune the size of Ca MNP at an almost constant rate of $-1.2$ nm/GPa. At 9.4 GPa, $CaF_2$ undergoes a structural phase transition from the fluorite to a contunnite phase, which is not superionic and displays an hexagonal cationic structure that is not compatible with the cubic symmetry of Ca nanocolloids[32,33]. Consequently, the formation of MNP is energetically not favourable (that is, the F centers cannot diffuse so to coalescence, and the creation of a sharp *fcc* Ca/contunnite $CaF_2$ interface is is not possible due to the incommesurability of the cation sublattices in the two involved structures) and the Ca nanocolloids vanish. This finding highlights the importance of chosing an appropriate ionic compound (i.e., with a cationic sublattice structure that is compatible with the resulting nanocolloid crystal symmetry) when employing our MNP size control method. Examples of materials in which our approach can be applied successfully include LiF, KF, $SrF_2$, and CsF, and numerous solid solutions involving similar binary compounds. Hence, our work should stimulate the design of new functional materials containing MNP with tailored dimensions for use in advanced optoelectronic and plasmonic applications.

# Acknowledgement

We thank Prof. A. Segura from the Universitat de València for his help during the experiments and Prof. K. Schwartz and C. Trautmann from the GSI Helmholtzzentrum für Schwerionenforschung for providing the irradiated samples of $CaF_2$. J.R.-F. and V.M. acknowledge the Spanish Ministry of Science, Innovation, and Universities for the Juan de la Cierva program IJCI-2014-20513, and FJCI-2016-27921, respectively. C.C. acknowledges

support from the Australian Research Council under the Future Fellowship funding scheme (No. FT140100135). Computational resources and technical assistance were provided by the Australian Government and the Government of Western Australia through the National Computational Infrastructure (NCI) and Magnus under the National Computational Merit Allocation Scheme and The Pawsey Supercomputing Centre. This project has received funding from the European Union's Horizon 2020 research and innovation programme under grant agreement No 829161.

# References

(1) Lohse, S. E.; Murphy C. J. Applications of Colloidal Inorganic Nanoparticles: From Medicine to Energy. *J. Am. Chem. Soc.* **2012**, *134*, 15607–15620.

(2) Puntes, V. F.; Krishnan, K. M.; Alivisatos, P. Colloidal Nanocrystal Shape and Size Control: The Case of Cobalt. *Science* **2001**, *291*, 2115–2117.

(3) Wuithschick, M.; Paul, B.; Bienert, R.; Sarfraz, A.; Vainio, U.; Sztucki, M.; Kraehnert, R.; Rademann, K.; Emmerling, F.; and Polte J. Size-Controlled Synthesis of Colloidal Silver Nanoparticles Based on Mechanistic Understanding. *Chem. Mater.* **2013**, *25*, 4679–4689.

(4) Link, S.; Masiello D. J. Introduction: Plasmonics in Chemistry. *Chem. Rev.* **2018**, *118*, 2863–2864.

(5) Alencar, O.; Ruiz-Fuertes, J.; Schwartz, K.; Trautmann, C.; Bayarjargal, L.; Haussühl, E.; Winkler B. Irradiation Effects in $CaF_2$ Probed by Raman Scattering. *J. Raman Spec.* **2016**, *47*, 978–983.

(6) Abedini, A.; Daud, A. R.; Abdul Hamid, M. A.; Kamil Othman, N.; Saion, E. A Review on Radiation-Induced Nucleation and Growth of Colloidal Metallic Nanoparticles. *Nanoscale Res. Lett.* **2013**, *8*, 474.

(7) Mankiewich, P. M.; Craighead, H. G.; Harrison, T. R.; Dayem, A. H. High Resolution Electron Beam Lithography on $CaF_2$. *Appl. Phys. Lett.* **1984**, *44*, 468.

(8) Cramer, L. P.; Schubert, B. E.; Petite, P. S.; Langford, S. C.; Dickinson, J. T. Laser Interactions with Embedded Ca Metal Nanoparticles in Single Crystal $CaF_2$. *J. Appl. Phys.* **2005**, *97*, 074307.

(9) Cramer, L. P.; Langford, S. C.; Dickinson, J. T. The Formation of Metallic Nanoparticles in Single Crystal $CaF_2$ under 157nm excimer laser irradiation. *J. Appl. Phys.* **2006**, *99*, 054305.

(10) Rix, S.; Natura, U.; Loske, F.; Letz, M.; Felser, C.; Reichling, M. Formation of Metallic Colloids in $CaF_2$ by Intense Ultraviolet Light. *Appl. Phys. Lett.* **2011**, *99*, 261909.

(11) Chadderton, L. T.; Johnson, E.; Wohlenberg, T. A Mechanism for the Formation of an Ordered Void Array on the Anion Sublattice in Fluorite. *Radiat. Eff. Defects Solids*, **1976**, *28*, 111–112.

(12) Kotomin, E. A.; Kuzovlov, V. N.; Popov, A. I. The Kinetics of Defect Aggregation and Metal Colloid Formation in Ionic Solids under Irradiation. *Radiat. Eff. Defects Solids* **2001**, *155*, (113–125).

(13) Bennewitz, R.; Reichling, M.; Wilson, R. M.; Williams, R. T.; Holldack, K.; Grunze, M.; Matthias, E. Characterization of Ca Aggregates on $CaF_2$ (111)-Surfaces by Atomic Force, XPS, and Fluorescence Microscopy. *Nucl. Instr. and Meth. B* **1994**, *91*, 623–627.

(14) Bennewitz, R.; Günter, C.; Reichling, M.; Matthias, E.; Vijayalakshmi, S.; Barmes, A. V.; Tolk, N. H. Size Evolution of Low Energy Electron Generated Ca Colloids in $CaF_2$. *Appl. Phys. Lett.* **1995**, 66, 320.

(15) Reichling, M.; Wilson, R. M.; Bennewitz, R.; Williams, R. T.; Gogoll, S.; Stenzel, E.; Matthias, E. Surface Colloid Evolution During Low-Energy Electron Irradiation of $CaF_2$(111). *Surf. Sci.* **1996**, *366*, 531–544.

(16) Bennewitz, R.; Smith, D.; Reichling, M. Bulk and Surface Processes in Low-Energy-Electron-Induced Decomposition of $CaF_2$. *Phys. Rev. B* **1999**, *59*, 8237.

(17) Tsujibayashi, T.; Toyoda, K.; Sakuragi, S.; Kamada, M.; Itoh, M. Spectral Profile of the Two-Photon Absorption Coefficients in $CaF_2$ and $BaF_2$. *Appl. Phys. Lett.* **2002**, *80*, 2883.

(18) Peng, Y.; Cheng, Z.; Zhang, Y.; Qiu, J. Laser-Induced Temperature Distribution and Thermal Deformation in Sapphire, Silicon, and Calcium Fluoride Substrates at 1.315 $\mu$m. *Opt. Eng.* **2001**, *40*, 2822–2829.

(19) Borchardt, J.K. Building Functional Materials Layer by Layer: Conference Report. *Mater. Today* **2005**, *8*, 18.

(20) Kaiser, U.; Kaiser, N.; Weissbrodt, P.; Mademann, U.; Hacker, E.; Müller, H. Structure of Thin Fluoride Films Deposited on Amorphous Substrates. *Thin Solid Films* **1992**, *217*, 7–16.

(21) Orena, V. M.; Alcalá, R. Formation and Size Evolution of Ca Colloids in Additively Colored $CaF_2$. *Phys. Stat. Sol (a)* **1976**, *38*, 621–627.

(22) Orena, V. M.; Alcalá, R. Optical Properties of Cation Colloidal Particles in $CaF_2$ and $SrF_2$. *Phys. Stat. Sol (a)* **1977**, *44*, 717–723.

(23) Orena, V. M.; Alcalá, R. Photothermal Bleaching of Ca Colloids in Additively Colored $CaF_2$. *Solid State Comm.* **1978**, *27*, 1109–1112.

(24) Natura, U.; Rix, S.; Letz, M.; Parthier, L. Study of Haze in 193 nm High Dose Irradiated $CaF_2$ Crystals. *Proc. SPIE* **2009**, *7504*, 75041P.

(25) Ma, Y.; Rohlfing, M. Optical Excitation of Deep Defect Levels in Insulators within Many-Body Perturbation Theory: The F Center in Calcium Fluoride. *Phys. Rev. B* **2008**, *77*, 115118.

(26) Geward, L.; Olsen, J. S.; Steentrup, S.; Malinowski, M.; Asbrink, S.; Waskowska, A. X-Ray Diffraction Investigations of $CaF_2$ at HIgh Pressure. *J. Appl. Crys.* **1992**, *25*, 578.

(27) Cazorla, C.; Errandonea, D. High-Pressure, High-Temperature Phase Diagram of Calcium Fluoride from Classical Atomistic Simulations. *J. Phys. Chem. C* **2013**, *117*, 11292–11301.

(28) Schmidt, E. D. D.; Vedam, K. Variation of the Refractive Indices of $CaF_2$, $BaF_2$ and $\beta$-$PbF_2$ with Pressure to 7 kbar. *J. Phys. Chem. Solids* **1966**, *27*, 1563–1566.

(29) Laven, P. Simulation of Rainbows, Coronas, and Glories by use of Mie Theory. *Appl. Optics* **2008**, *42*, 436–444.

(30) Bohren, C. F.; Huffman, D. R., *Absorption and Scattering of Light by Small Particles* (Wiley-Interscience, Hoboken, NJ, USA, 1983).

(31) Cazorla, C.; Errandonea, D. Giant Mechanocaloric Effects in Fluorite-Structured Superionic Materials. *Nano Lett.* **2016**, *16*, 3124–3129.

(32) Cazorla, C.; Sagotra, A. K.; King, M.; Errandonea, D. High-Pressure Phase Diagram and Superionicity of Alkaline Earth Metal Difluorides. *J. Phys. Chem. C* **2018**, 122, 1267–1279.

(33) Cazorla, C.; Errandonea, D. Superionicity and Polymorphism in Calcium Fluoride at High Pressure. *Phys. Rev. Lett.* **2014**, *113*, 235902.

(34) Yang, J. X.; Zhao, H. L.; Gong, H. R.; Song, M.; Ren, Q. Q. Proposed Mechanism

of *hcp*$\longrightarrow$ *fcc* Phase Transition in Titanium through First Principles Calculation and Experiments. *Sci. Reports.* **2018**, *8*, 1992.

(35) Weerkamp, J. R. W.; Groote, J. C.; Seinen, J.; den Hartog, H. W. Radiation Damage in NaCl. I. Optical-Absorption Experiments on Heavily Irradiated Samples. *Phys. Rev. B* **1994**, *50*, 9781.

(36) Pizzini, S. Ionic Conductivity in Lithium Compounds. *J. Appl. Electrochem.* **1972**, *1*, 153–161.

(37) Olinger, B.; Shaner, J. W. Lithium, Compression and High-Pressure Structure. *Science* **1983**, *219*, 1071–1072.

(38) Liu, L.-G. Compression and Polymorphism of Potassium to 400 kbar. *J. Phys. Chem. Solids* **1986**, *47*, 1067–1072.

(39) Olinger, B.; Weddeling, F. K. A Pressure-Induced fcc-to-bcc Transformation in Strontium. *J. Appl. Phys.*, **1965**, *36*, 328.

(40) Pistorius, C.; Snyman, H. Polymorphism of the Alkali Metal Fluorides at High Pressures. *Z. Physik Chem. N.F.* **1964**, *43*, 1.

(41) Hall, H. T.; Mernill, L.; Barnett, J. D. High Pressure Polymorphism in Cesium. *Science* **1964**, *146*, 1297–1299.

(42) Mao, H. K.; Bell, P. M.; Shaner, J. W.; Steinberg D. J. Specific Volume Measurements of Cu, Mo, Pd, and Ag and Calibration of the Ruby R1 Fluorescence Pressure Gauge from 0.06 to 1 Mbar. *J. Appl. Phys.* **1978**, *49*, 3276.

(43) Kresse, G.; Furthmüller, J. Efficient Iterative Schemes for *ab initio* Total-Energy Calculations Using a Plane-Wave Basis Set. *Phys. Rev. B* **1996**, *54*, 11169.

(44) Perdew, J. P.; Burke, K.; Ernzerhof, V. Generalized Gradient Approximation Made Simple. *Phys. Rev. Lett.* **1996**, *77*, 3865.

(45) Blöchl, P. E. Projector Augmented-Wave Method. *Phys. Rev. B* **1994**, *50*, 17953.

# Graphical TOC Entry